



# Cu(II)-influenced adsorption of ciprofloxacin from aqueous solutions by magnetic graphene oxide/nitrilotriacetic acid nanocomposite: Competition and enhancement mechanisms

Mei-fang Li <sup>a,b</sup>, Yun-guo Liu <sup>a,b,\*</sup>, Shao-bo Liu <sup>c,\*</sup>, Ding Shu <sup>d</sup>, Guang-ming Zeng <sup>a,b</sup>, Xin-jiang Hu <sup>e,f</sup>,  
Xiao-fei Tan <sup>a,b</sup>, Lu-hua Jiang <sup>a,b</sup>, Zhi-li Yan <sup>a,b</sup>, Xiao-xi Cai <sup>a,b</sup>

<sup>a</sup> College of Environmental Science and Engineering, Hunan University, Changsha 410082, PR China

<sup>b</sup> Key Laboratory of Environmental Biology and Pollution Control (Hunan University), Ministry of Education, Changsha 410082, PR China

<sup>c</sup> School of Metallurgy and Environment, Central South University, Changsha 410083, PR China

<sup>d</sup> Light Alloy Research Institute, Central South University, Changsha 410083, PR China

<sup>e</sup> College of Environmental Science and Engineering, Central South University of Forestry and Technology, Changsha 410004, PR China

<sup>f</sup> College of Natural Resources and Environment, South China Agricultural University, Guangzhou 510642, PR China

## HIGHLIGHTS

- NDMGO is synthesized by nitrilotriacetic acid and magnetic graphene oxide.
- Sorption kinetic, isothermal and thermodynamic characteristics of CIP are studied.
- Cu obviously enhances the CIP adsorption capability through Cu bridging effect.
- Ionic strength, foreign ions and addition sequences of CIP/Cu are investigated.
- Hydrogen bond, electrostatic and  $\pi$ - $\pi$  interaction are involved in the mechanism.

## ARTICLE INFO

### Article history:

Received 22 December 2016

Received in revised form 3 March 2017

Accepted 6 March 2017

Available online 8 March 2017

### Keywords:

Ciprofloxacin

Cu(II)

Magnetic graphene oxide

Nitrilotriacetic acid

Adsorption mechanism

## ABSTRACT

Nitrilotriacetic acid-functionalized magnetic graphene oxide (NDMGO) was developed for the removal of ciprofloxacin (CIP) with and without the presence of Cu(II). The physicochemical properties of NDMGO were characterized using SEM, TEM, XRD, FT-IR, XPS and zeta potential measurements. The CIP adsorption process could be better simulated by the pseudo-second-order kinetics and Freundlich isotherm model. Effects of Cu(II) concentrations on CIP uptake, as well as the influence of pH, ionic strength, background electrolyte and the addition sequences of CIP/Cu(II) were investigated. Adsorption results exhibited that the presence of Cu(II) obviously enhanced the CIP adsorption capability through Cu(II) bridging effect. The adsorption capacity for CIP was stronger in the (CIP-Cu(II))-NDMGO system than in the (NDMGO-Cu(II))-CIP and (NDMGO-CIP)-Cu(II) systems. Meanwhile, this nanomaterial showed high performance for Cu(II) adsorption. In addition to Cu(II) bridge enhancement, the mechanism could also be explained by hydrogen bonds, amidation reaction, electrostatic and  $\pi$ - $\pi$  interaction. These results provided valuable information for the removal of CIP and improved our understanding on reaction mechanism of antibiotics by NDMGO in the presence of metal ions, demonstrated that NDMGO could be developed as an effective adsorbent to simultaneously removal metal ions and organic substances.

© 2017 Elsevier B.V. All rights reserved.

\* Corresponding authors at: College of Environmental Science and Engineering, Hunan University, Changsha 410082, PR China (Y.-g. Liu), School of Metallurgy and Environment, Central South University, Changsha 410083, PR China (S.-b. Liu).

E-mail addresses: [liuyunguo\\_hnu@163.com](mailto:liuyunguo_hnu@163.com) (Y.-g. Liu), [liushaobo23@aliyun.com](mailto:liushaobo23@aliyun.com) (S.-b. Liu).

## 1. Introduction

As a synthetic fluoroquinolone antibacterial, ciprofloxacin (CIP) is widely used for treating bacterial infection in humans and animals, resulting in frequent detected in the aquatic environment [1]. Owing to the bacteria-inhibiting effect, the CIP residues are very hard to remove by traditional waste water treatment plants (WWTP) [2], which may pose potential threats to the ecosystem

and human health via the induction proliferation of antibiotic resistant genes [3]. Therefore, the persistence of CIP in the environment has attracted increasingly significant environmental concern. Even so, few researches on the high-efficiency elimination of CIP have been reported compared with other antibiotics [2].

In the present study, adsorption is proved to be a simple, economical and efficient method to remove antibiotics from wastewaters [2,4]. Various adsorbents have been explored for the adsorption of CIP, such as montmorillonite [5], biochar [6,7], activated carbon [2], carbon nanotubes [8], and goethite [9]. However, these adsorbents hold poor potential for CIP removal, such as low sorption capacities, high cost or poor regeneration performance. In a previous study, we had synthesized a magnetic composite adsorbent by reacting nitrilotriacetic acid to magnetic graphene oxide through diethylenetriamine [10]. This adsorbent was found to be an ideal adsorbent for tetracycline removal because it had a lot of amino and carboxyl groups, which could effectively combine with the amine and hydroxyl groups of tetracycline. The oxygen-containing and nitrogen-containing functional groups also had a relatively high reactivity and easily bonded with the carboxyl groups and  $\pi$ -electrons of the CIP. Besides, it could realize the retrieval and separation from the medium rapidly and effectively by a magnet. Therefore, this aminated magnetic graphene oxide composite (NDMGO) might be an ideal adsorbent to develop for CIP removal.

In general, the water body is a complex system where antibiotics and metal ions often coexist in wastewater [11], and metal ions can react with antibiotics, thus influencing the removal of antibiotics [2]. Copper (Cu(II)) is one of the harmful heavy metal ions. When the ingestion of copper beyond the regulation limit of 1.3 mg/L [12], it can cause liver and kidneys damage and lung cancer in humans [12,13]. In natural waters, the presence of Cu (II) has strong complexation ability with antibiotics and plays an important role in antibiotics removal. Wang et al. [14] and Pei et al. [5] were reported that Cu(II) can form ions bridge with antibiotics, thereby influencing the removal of antibiotics. Although some previous studies have given some insights into the antibiotics removal as affected by heavy metals, more research are considerable practical to better understand the influence mechanism.

The objectives of this study were to (i) understand the adsorption behavior of CIP onto NDMGO; (ii) probe the effects of Cu(II) concentration and addition sequences on CIP adsorption; (iii) investigate the effects of various solution properties, such as solution pH, ionic strengths and background electrolytes on CIP/Cu(II) removal on NDMGO; (iiii) discuss the major sorption mechanisms of CIP onto NDMGO as affected by Cu(II) with the characterization analysis.

## 2. Materials and methods

### 2.1. Materials

Graphite powder, nitrilotriacetic acid (NTA), diethylenetriamine were supplied by Sinopharm Chemical Reagent Co., Ltd., China. Ciprofloxacin (CIP) used as adsorbate was obtained from Hefei Bomei Biotechnology Co., Ltd., China. A stock solution of Cu(II) was prepared by dissolving exact quantities of 1 g in 1 L deionized water. All other chemicals used in the experiments were analytical grade.

### 2.2. Synthesis of NDMGO

Graphene oxide (GO) was synthesized by oxidizing natural graphite powder based on modified Hummers's method [15,16]. Generally, 6 g graphite powder, 5 g  $K_2S_2O_8$  and 5 g  $P_2O_5$  were added into

24 mL 98%  $H_2SO_4$  and stirred at a temperature of 80 °C for 4.5 h. The mixture was washed with deionized water till solution became neutral and dried under vacuum at 60 °C. Next, the obtained pre-oxidized graphite was poured into the mixture of 240 mL cold (0 °C)  $H_2SO_4$ , 30 g  $KMnO_4$  and 5 g  $NaNO_3$  under stirring and the reaction temperature was kept below 20 °C for 4 h. Then the mixtures were heated to 35 °C for 2 h and 98 °C for 1 h. After that, 40 mL of 30%  $H_2O_2$  was added to eliminate the excess  $MnO_4^{2+}$  and the resulting material was rinsed with HCl solution (10%) and deionized water. The preparation procedure of magnetic graphene oxide (MGO) was reported in previous study [17,18]. Concisely,  $Fe^{3+}$  and  $Fe^{2+}$  (molar ratio 2:1) were mixed in the GO suspension with addition of ammonia solution to form  $Fe_3O_4$ -GO composite (MGO). Subsequently, nitrilotriacetic acid-functionalized magnetic graphene oxide (NDMGO) was obtained by reacting NTA with MGO through diethylenetriamine using previous method [10]. The obtained NDMGO was rinsed with deionized water until the solution was neutral, then stored at room temperature.

### 2.3. Sorption experiments

All batch adsorption experiments were carried out in 25 mL clear conical flasks by adding 2.5 mg NDMGO with a shaking speed of 150 rpm. The suspension pH values were adjusted using negligible volumes of 0.01–0.1 mol/L HCl and NaOH solutions. A standard stock solution of CIP used in batch experiments was prepared by dissolving 1 g of CIP powder into 1 L hydrochloric acid solution. The desired CIP and Cu(II) concentrations used in this experiment were obtained by diluting the stock solution. In order to investigate the effect of contact time on CIP adsorption, 50 mg/L CIP was analyzed at 0–24 h and pH 9.0. For the equilibrium adsorption and thermodynamic experiments, the initial concentrations of CIP were in the range of 10–100 mg/L and the experimental temperatures were controlled at 283, 298, and 313 K, respectively (pH was 6.0 due to high concentration of CIP was easy to precipitate at pH 9.0). The solid/liquid phases were separated by a permanent magnet. The experimental data were reported as the average of three duplicate experiments.

### 2.4. Adsorption of CIP onto NDMGO as affected by Cu(II)

The effect of pH on adsorption of CIP onto NDMGO with and without Cu(II) was conducted as follows: In this research, 50 mg/L CIP was employed as the adsorbate to examine the sorption behavior by the NDMGO at pH 3.0–11.0. CIP adsorption with three different Cu(II) concentrations (0.01, 0.1 and 1.0 mg/L, respectively) were conducted at pH ranging from 3.0 to 11.0.

The effect of Cu(II) concentration on adsorption of CIP onto NDMGO was conducted as follows: 2.5 mg NDMGO was added into 50 mg/L of CIP with different concentrations (0, 0.01, 0.1, 0.5, 1.0, 2.0, 3.0, 4.0, 8.0 and 10.0 mg/L) of Cu(II) at pH 9.0 and 298 K.

The effects of ionic strength and background electrolytes on adsorption of CIP onto NDMGO were realized as follows: 0–1.0 mol/L NaCl and 0–0.1 mol/L four foreign ions ( $K^+$ ,  $Ca^{2+}$ ,  $SO_4^{2-}$  and  $NO_3^-$ ) were added into 50 mg/L CIP solutions (pH 9.0) in the presence or absence of Cu(II), respectively.

The effects of addition sequences on the sorption of CIP and Cu (II) onto NDMGO were investigated at pH ranging from 3.0 to 11.0. The three addition sequences were as follows: (1) NDMGO and 10 mg/L Cu(II) at pH 3.0–11.0 were pre-equilibrated for 14 h before the addition of CIP (named as (NDMGO-Cu)-CIP); (2) NDMGO and 50 mg/L CIP at pH 3.0–11.0 were pre-equilibrated for 14 h before the addition of Cu(II) (named as (NDMGO-CIP)-Cu); (3) The mixture of 50 mg/L CIP and 10 mg/L Cu(II) at pH 3.0–11.0 were pre-equilibrated for 14 h before the addition of NDMGO (named as (CIP-Cu)-NDMGO).

## 2.5. Adsorbent characterization

Scanning electron microscopy (SEM) (Hitachi S-4800, Japan) and transmission electron microscopy (TEM) (Tecnai G2 F20, USA) images were used to determine the structure and morphology of NDMGO. The X-ray diffraction (XRD) pattern of NDMGO was carried out using a Bruker D8-Advance X-ray diffractometer (Bruker, German). The Fourier transform infrared (FTIR) spectra of GO, MGO, NDMGO, NDMGO-Cu, and CIP treated NDMGO with and without Cu(II) were recorded on a Nicolet 6700 spectrophotometer. X-ray photoelectron spectroscopy (XPS) analysis was conducted based on an ESCALAB 250Xi spectrometer (Thermo Fisher, USA). The zeta potentials of NDMGO in 0–0.01 mol/L NaCl solution with and without 10 mg/L Cu(II) were measured at different pH using a zeta potential meter (Zetasizer Nano-ZS90, Malvern).

## 2.6. CIP and Cu(II) detection

The concentration of CIP in supernatant solution was analyzed by an UV-Vis spectrophotometer (UV-2550, SHIMADZU, Japan) at the maximum absorption wavelength of 275 nm [19] and Cu(II) by flame atomic absorption spectrometry (PerkinElmer AA700, USA). The quantity of CIP or Cu(II) adsorbed ( $q_e$ ) was calculated using the following equation:

$$q_e = \frac{(C_0 - C_e)V}{m} \quad (1)$$

where  $C_0$  and  $C_e$  (mg/L) are the initial and equilibrium CIP or Cu(II) concentrations, respectively;  $V$  (L) is the initial volume of the CIP or Cu(II) solution, and  $m$  (g) is the mass of the adsorbent used.

## 3. Results and discussion

### 3.1. Characterization of NDMGO

To investigate the morphology and structure of this modified material, SEM and TEM images are conducted and illustrated in Fig. 1a and b, respectively. As shown in Fig. 1a, many wrinkles were distributed on the surface of NDMGO after modification, which

might be due to the grafting of magnetic nanoparticles and NTA. The further proof was provided by TEM image of this nanocomposite (Fig. 1b). It revealed that many nanoparticles were dispersed on the GO surface, which was ascribed to the introduction of  $\text{Fe}_3\text{O}_4$  nanoparticles [20]. The XRD pattern of NDMGO is presented in Fig. 1c. It was known that the composite exhibited seven strong characteristic peak at 30.19, 35.61, 37.06, 43.15, 53.79, 57.37 and 62.99° (2 $\theta$ ), which were consistent with the (220), (311), (222), (400), (422), (511) and (440) facets of the cubic spinel crystal planes of  $\text{Fe}_3\text{O}_4$  (JCPDS 19-0629), respectively [21]. Based on the XRD result, it could be concluded that the NTA binding did not cause the crystalline phase change of the magnetic nanoparticles [22].

The FT-IR spectra of GO, MGO, and NDMGO are presented in Fig. 1d. From Fig. 1d, the absorption bands of GO appeared at 3462, 1628, 1391, and 1066  $\text{cm}^{-1}$  attributed to the skeletal vibration of O–H, C=C, O=C–O and C–O bonds, respectively [3,23]. Similar functional groups above mentioned were also found in MGO, but with the presence of strong peak at 566  $\text{cm}^{-1}$  for Fe–O [24], confirming that a large number of  $\text{Fe}_3\text{O}_4$  particles were successfully loaded on the GO surface. In comparison to the peaks of functional groups of MGO, a new characteristic peak of NDMGO at 1458  $\text{cm}^{-1}$  was assigned to the vibration of –NHCO– [24], which suggested successful synthesis of NDMGO and possible connection of NTA and MGO through –NHCO– bond.

### 3.2. Kinetics of CIP adsorption

The effect of contact time on adsorption of CIP onto NDMGO is investigated and the resulting kinetic plots are displayed in Fig. 2a. CIP adsorption by NDMGO increased rapidly at first, then slowed down gradually, and finally reached the maximum adsorption capacity at approximately 14 h.

To understand the time dependent removal of CIP by NDMGO, the widely used kinetics models, pseudo-first and second-order models were used to fit the experiment data. Detailed information about these models was described in the Supplementary Materials. Linearized fitting forms about these models are illustrated in Fig. 2b. The parameters and the correlation coefficient values of

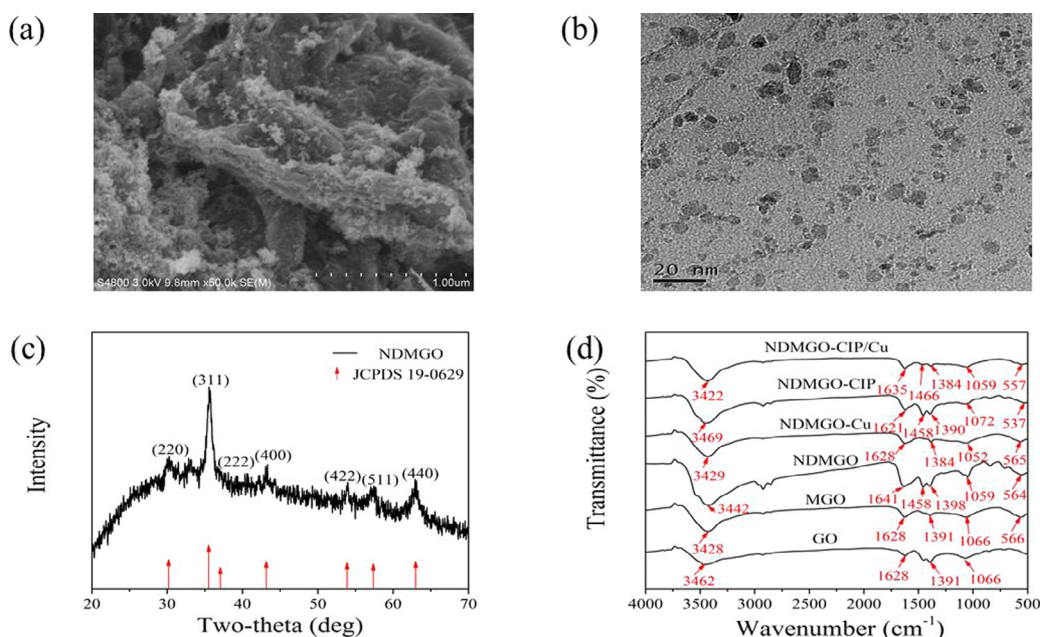


**Fig. 1.** (a) SEM image of NDMGO; (b) TEM image of NDMGO; (c) XRD pattern of NDMGO; (d) FT-IR spectra of GO, MGO, NDMGO, NDMGO-Cu, NDMGO-CIP, and NDMGO-CIP/Cu.

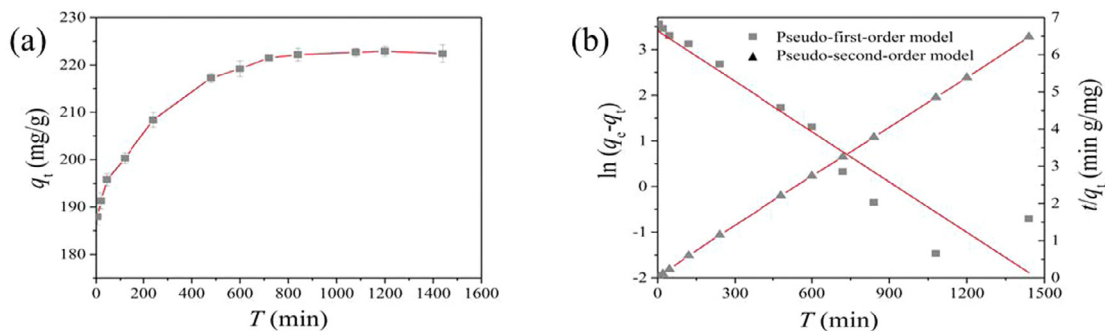


**Fig. 2.** (a) Effect of contact time on the adsorption of CIP; (b) The pseudo-first-order and pseudo-second-order kinetics models.  $C_{0(\text{CIP})} = 50 \text{ mg/L}$ ,  $m/V = 0.10 \text{ g/L}$ ,  $T = 25 \text{ }^\circ\text{C}$ ,  $\text{pH} = 9.0$ .

different kinetic models are presented in Table 1. In comparison to the pseudo-first-order model, the correlation coefficient for the pseudo-second-order kinetic model was higher than 0.999, moreover, the calculated  $q_e$  values generated by pseudo-second-order kinetic model was more identical with the experimental data. It can be seen that the sorption kinetics could be well explained by pseudo-second-order kinetic model, which indicated the rate-limiting step of the adsorption process was controlled by chemisorption [25].

### 3.3. CIP adsorption isotherm and thermodynamics

To gain insights into the CIP adsorption mechanism onto NDMGO, two frequently used isotherm models (Langmuir and Freundlich) were employed to fit the adsorption equilibrium data. Langmuir model can be applied to elucidate homogeneous adsorption systems where adsorption is a monolayer reaction took place on a homogeneous adsorption sites. Whereas the Freundlich equation is proposed as an empirical equation implying that the adsorption is a multilayer heterogeneous adsorption [26]. The equations of Langmuir and Freundlich models could be found in the Supplementary Materials.

Two adsorption isotherms of CIP on NDMGO are provided in Fig. 3. The corresponding parameters calculated from the two adsorption models at three different temperatures are summarized in Table 2. As can be seen, by comparing the value of correlation coefficients ( $R^2$ ), root mean square error (RMSE) and chi-square test ( $\chi^2$ ), it was clear that the Freundlich model could describe the adsorption data better than the Langmuir model. This phenomenon confirmed that a multilayer heterogeneous coverage of CIP on the interface of the material was formed.

To investigate more about adsorption characteristics of CIP on NDMGO, the thermodynamic analysis was performed. The thermodynamic parameters ( $\Delta G^\circ$ ,  $\Delta H^\circ$ , and  $\Delta S^\circ$ ) are calculated from the temperature-dependent sorption isotherms via relative equations (presented in the Supplementary Materials) and tabulated in Table 3. From Table 3, the negative values of  $\Delta G^\circ$  indicated that this adsorption involved a favorable and spontaneous process. The positive values of  $\Delta H^\circ$  reflected the typical endothermic nature of adsorption process of CIP on NDMGO, which was suggested by the study for effect of temperature. Compared with the movement of CIP in aqueous solution, the movement of CIP absorbed on

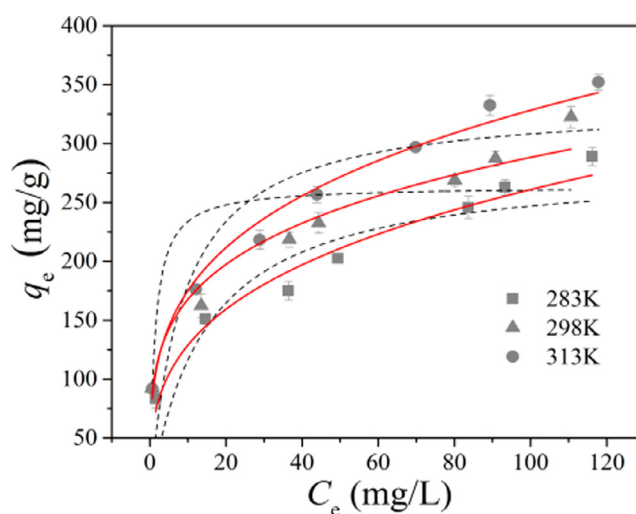


**Fig. 3.** Langmuir and Freundlich models for the adsorption of CIP by NDMGO at different temperatures (the solid lines and dotted lines are the Freundlich and Langmuir model simulation, respectively).  $m/V = 0.10 \text{ g/L}$ ,  $\text{pH} = 6.0$ ,  $t = 14 \text{ h}$ .

NDMGO was more easier, which was supported by the positive values of  $\Delta S^\circ$  [27].

### 3.4. Effect of pH and Cu(II) concentration

Solution pH can change the speciation of adsorbate and surface functional groups on adsorbent, thus it is essential to study the pH effect on the sorption process [28]. Sorption of CIP on NDMGO at solution pH 3.0–11.0 is investigated in the presence and absence of Cu(II) and shows in Fig. 4a. As seen from Fig. 4a, the removal efficiency of CIP first increased and then decreased with increasing the pH. The maximum amount of CIP was 230.57 mg/g, which was occurred at about pH 9.0. The  $\text{pK}_a$  values ( $\text{pK}_a = 5.90$  and 8.89) of CIP suggest that the CIP exists in cation, zwitterion and anion forms at different pH values [29] and its ionic forms with solution pH are performed in Fig. S1. The zeta potentials of NDMGO have been detected and present in Fig. 6. At  $\text{pH} < 6.0$ , the principal species of CIP was  $\text{CIP}^+$  and the electrostatic repulsion between  $\text{CIP}^+$  and positively charged material surface made further sorption unfavor-

**Table 1**  
Model results of CIP adsorption kinetics data.

$q_{e,\text{exp}}$		Pseudo-first-order		Pseudo-second-order		
222.88	$k_1$ (1/min)	$q_{e,1}$ (mg/g)	$R^2$	$k_2$ (g/mg min)	$q_{e,2}$ (mg/g)	$R^2$
	$3.67 \times 10^{-3}$	30.15	0.903	$4.99 \times 10^{-4}$	223.71	>0.999

**Table 2**  
Langmuir and Freundlich isotherm parameters for adsorption of CIP on NDMGO.

Isotherms	Parameters	Temperature (K)		
		283	298	313
Langmuir	$q_m$ (mg/g)	282.06	263.78	334.78
	$K_L$ (L/mg)	0.07	0.78	0.12
	$R^2$	0.76	0.86	0.78
	RMSE	4.92	5.85	9.46
	$\chi^2$	24.23	34.27	89.47
Freundlich	$K_f$ [(mg/g)/(mg/L) <sup>N</sup> ]	63.59	97.48	93.34
	N	0.31	0.24	0.27
	$R^2$	0.96	0.99	0.99
	RMSE	1.91	1.89	1.89
	$\chi^2$	3.66	3.56	3.56

**Table 3**  
Thermodynamic parameters for adsorption of CIP on NDMGO.

T (K)	$\ln K_0$	$\Delta G^\circ$ (kJ/mol)	$\Delta H^\circ$ (kJ/mol)	$\Delta S^\circ$ (J/K mol)
283	1.09	-2.56	3.69	0.022
298	1.26	-3.12		
313	1.24	-3.23		

able. In the pH range of 6.0–9.0, CIP removal increased with increasing of pH and reached a maximum at pH around 9.0. The main species presented in this pH range were  $\text{CIP}^{\pm}$ , which could easily be adsorbed on the negatively charged NDMGO surfaces. At  $\text{pH} > 9.0$ ,  $\text{CIP}^-$  began to form, but adsorption of this species on the negatively charged surfaces of NDMGO was difficult, resulting in the decrease of adsorption amounts.

After the addition of Cu(II) to the solution, there was a distinct effect on the removal of CIP onto NDMGO over the tested pH range of 3.0–11.0. When CIP and low concentration Cu(II) (0.01 mg/L) were present together at  $\text{pH} < 7.0$ , the sorption amounts of CIP

slightly weaken in comparison with single CIP adsorption. It was possibly because that the main speciation in the suspension was  $\text{Cu}^{2+}$ ,  $\text{Cu}_2(\text{OH})_2^{2+}$ ,  $\text{CuOH}^+$ , and  $\text{CIP}^+$  (Figs. S1 and S2) and the phenomenon of competitive adsorption were existed among these species, thus more hardly adsorbed on the positively charged surface of NDMGO than  $\text{CIP}^+$ . While the solution pH was above 7.0, low concentration Cu(II) exerted slight positive effect on the CIP sorption owing to the formation of metal hydroxide, such as  $\text{Cu}(\text{OH})_2(\text{s})$ . The  $\text{Cu}(\text{OH})_2(\text{s})$  could act as adsorbents for the adsorption of CIP from the solution [30]. With the Cu(II) concentration increased to 0.1 and 1.0 mg/L, the promotion effect became stronger in the pH range of 3.0–11.0, which could be ascribed to the formation of Cu(II) bridge [5] between CIP and NDMGO.

The adsorption of Cu(II) on NDMGO was also examined in the pH range of 3.0 to 11.0 to ascertain the optimal pH of coadsorption. As seen from Fig. S3, the sorption capacity of Cu(II) increased with the increase of pH, and maintained at maximum adsorption capacity of 74.93 mg/g at  $\text{pH} \geq 9.0$ . Evidently,  $\text{pH} = 9.0$  was considered as the optimum pH for both of CIP and Cu(II) removal. Fig. 4b showed

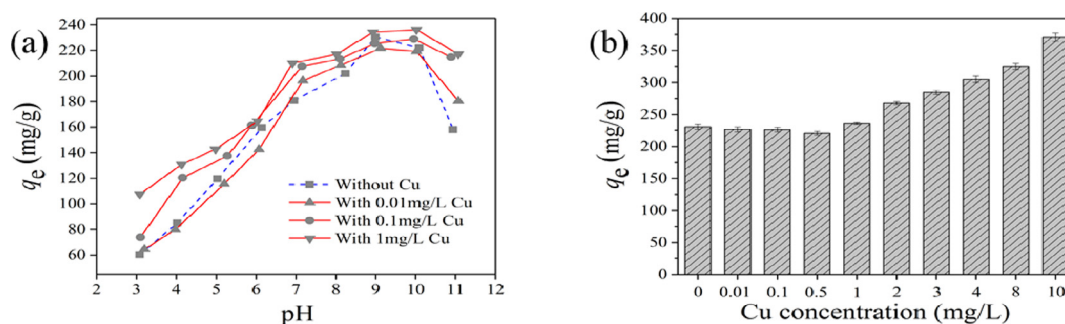


**Fig. 4.** (a) pH effect on CIP adsorption onto NDMGO with and without 0.01–1.0 mg/L Cu(II); (b) Effect of Cu(II) concentration on CIP adsorption at pH 9.0.  $C_{0(\text{CIP})} = 50$  mg/L,  $m/V = 0.10$  g/L,  $T = 25$  °C,  $t = 14$  h.

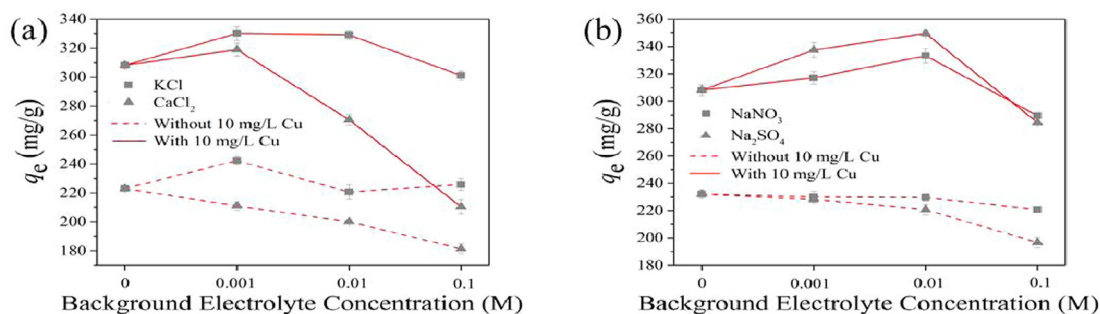


**Fig. 5.** Effects of background electrolytes on CIP adsorption by NDMGO with and without Cu(II) (a: foreign cations, b: foreign anions).  $C_{0(\text{CIP})} = 50$  mg/L,  $C_{0(\text{Cu})} = 10$  mg/L,  $m/V = 0.10$  g/L,  $T = 25$  °C,  $\text{pH} = 9.0$ ,  $t = 14$  h.

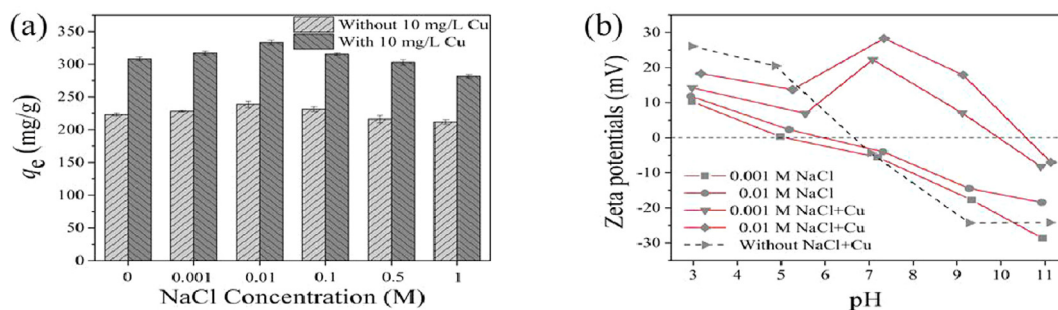


**Fig. 6.** (a) Effects of ionic strength on the adsorption of CIP by NDMGO with and without Cu(II) at pH 9.0; (b) Zeta potentials of NDMGO at different NaCl solution with and without Cu(II).  $C_{0(\text{CIP})} = 50 \text{ mg/L}$ ,  $C_{0(\text{Cu})} = 10 \text{ mg/L}$ ,  $m/V = 0.10 \text{ g/L}$ ,  $T = 25 \text{ }^\circ\text{C}$ ,  $t = 14 \text{ h}$ .

that the Cu(II) concentration significantly affected CIP uptake at pH = 9.0. CIP adsorption decreased slightly with increasing Cu(II) concentration from 0 to 0.5 mg/L, and increased with increasing Cu(II) concentration from 0.5 to 10 mg/L. When the initial concentration of Cu(II) was below 0.5 mg/L, the decrease of CIP adsorption could be interpreted by the competition of adsorption sites with Cu(II) on the NDMGO surface. As the concentration of Cu(II) increased, more Cu(II) ions produced a change in the packing, spacing, or alignment of adsorbed CIP [31]. The interactions between Cu(II) and NDMGO neutralized repulsive forces between NDMGO and CIP, thus creating favorable sorption sites [32].

### 3.5. Effect of ionic strength and background electrolytes

Several types of background electrolyte ion, such as  $\text{K}^+$ ,  $\text{Ca}^{2+}$ ,  $\text{NO}_3^-$  and  $\text{SO}_4^{2-}$ , are simultaneously present with pollutants in natural water or wastewater system, which can affect the removal of pollutants [33]. Fig. 5a and b exerted different effects of two foreign cations ( $\text{K}^+$  and  $\text{Ca}^{2+}$ ) and anions ( $\text{SO}_4^{2-}$  and  $\text{NO}_3^-$ ) on CIP adsorption with or without the presence of Cu(II), respectively. As depicted in Fig. 5a, the CIP removal capacity significantly decreased with the increase of  $\text{CaCl}_2$  concentration from 0 to 0.1 mol/L, however, the adsorption capacity of CIP first increased and then slightly decreased with the KCl concentration increasing from 0 to 0.1 mol/L. It confirmed that the effects of the divalent  $\text{Ca}^{2+}$  on CIP sorption were stronger than that of monovalent  $\text{K}^+$  with or without the presence of Cu(II). The result was similar to the cobalt(II) sorption on magnetite/graphene oxide [34], and these phenomena could be explained by two possible reasons: (i) The electrostatic attraction between the bivalent  $\text{Ca}^{2+}$  and adsorbent surface was stronger than that of the monovalent  $\text{K}^+$  [33]. (ii) One  $\text{K}^+$  adsorbed on the NDMGO surface only took up one adsorption site, while  $\text{Ca}^{2+}$  could occupy two sites [35], which contributed to a noticeable influence on the CIP uptake in the presence of  $\text{CaCl}_2$ .

From Fig. 5b, when adsorption occurred in the absence of Cu(II), the  $\text{NO}_3^-$  and  $\text{SO}_4^{2-}$  suppress the CIP removal but the inhibitory effect of  $\text{NO}_3^-$  could be negligible. This inhibition was probably due to the  $\text{NO}_3^-$  and  $\text{SO}_4^{2-}$  would occupy for limited adsorption sites. The promoting effect on CIP adsorption on the NDMGO was more obvious in 0–0.01 mol/L  $\text{Na}_2\text{SO}_4$  solution than in 0–0.01 mol/L  $\text{NaNO}_3$  solution in the presence of Cu(II) at pH 9.0. Lam et al. [36] pointed out that Cu(II) adsorption onto NDMGO required at least two sites and could not adsorb on the isolated sites.  $\text{SO}_4^{2-}$  was likely to act as one of the adsorption sites for Cu(II) adsorption [37], therefore enhancing the adsorption capacity for CIP through Cu(II) ions bridge. After the  $\text{NaNO}_3$  and  $\text{Na}_2\text{SO}_4$  concentration increased from 0.01 to 0.1 mol/L, the competition for the adsorption sites between  $\text{NO}_3^-$  or  $\text{SO}_4^{2-}$  and  $\text{CIP}^-$  might be stronger than ions bridge effect, thus the sorption capacity of CIP was gradually reduced.

The effect of ionic strength on the removal of CIP with the NDMGO composite was examined by carrying out a series of experiments at 0–1.0 mol/L NaCl solutions with or without the presence of Cu(II). According to the Fig. 6a, when the NaCl concentration was <0.01 M, the CIP sorption increased with the increasing NaCl concentration. The results might be related to the change of zeta potential of NDMGO surface. Fig. 6b presented the zeta potential of NDMGO surface in the NaCl solution with or without the presence of Cu(II) at pH from 3.0 to 11.0. From Fig. 6b, the surface charge of NDMGO was negative at pH 9.0, which was hard to combine with the negatively charged  $\text{CIP}^-$  because of the electrostatic repulsion. After NaCl adding into the system, the NDMGO surface was less negatively charged at pH 9.0 with the NaCl concentration increasing from 0 to 0.01 M, which was favorable to the adsorption of  $\text{CIP}^-$ . When both copper ions and NaCl coexisted in the solution, the negatively charged  $\text{CIP}^-$  were easily adsorbed by positively charged NDMGO, thus the CIP adsorption capacity increased tremendously in the presence of Cu(II) than the absence of Cu(II). At NaCl concentration >0.01 M, the adsorption of  $\text{CIP}^-$  on the surfaces of NDMGO became unfavorable. The main reason might be the competition of high-density salt solution with CIP for the available binding sites of NDMGO by a squeezing-out effect, resulting in the decrease of adsorption amounts of CIP [10].

### 3.6. Effect of addition sequences

Fig. 7 showed that a significant effect of all three CIP/Cu(II) addition sequences on CIP and Cu(II) adsorption by NDMGO at pH from 3.0 to 11.0. CIP and Cu(II) adsorption first increased and then remained at a high level with increasing pH. Fig. 7a demonstrated the differences in the mechanisms of CIP adsorption on NDMGO. In the (NDMGO-Cu(II))-CIP ternary system, Cu(II) and NDMGO were pre-equilibrated for 14 h before CIP was added, where the complexation between adsorbed Cu(II) and the CIP molecular in solution seemed difficult, and only a portion of the free Cu(II) ions could form complexes with CIP and then are adsorbed on NDMGO. In the (NDMGO-CIP)-Cu(II) ternary system, CIP had reached saturation adsorption after reaction with NDMGO. When Cu(II) was added to this suspension, strong complexation with the unremoved CIP molecular would improve the adsorption capacity of CIP in solution. We speculated that in the (CIP-Cu(II))-NDMGO ternary system, where Cu(II) was pre-equilibrated with CIP, most of the Cu(II) ions form complexes with CIP and then were adsorbed on NDMGO. Hence, in this system, the removal ability of CIP was strongest than the previous two cases.

The obvious differences of addition sequences on Cu(II) adsorption by NDMGO is shown in Fig. 7b. In the case of (NDMGO-CIP)-Cu(II), CIP first adsorbed on NDMGO would take up some of the adsorption sites of NDMGO surfaces, which was not conducive to the adsorption of Cu(II). However, in the (NDMGO-Cu(II))-CIP sys-

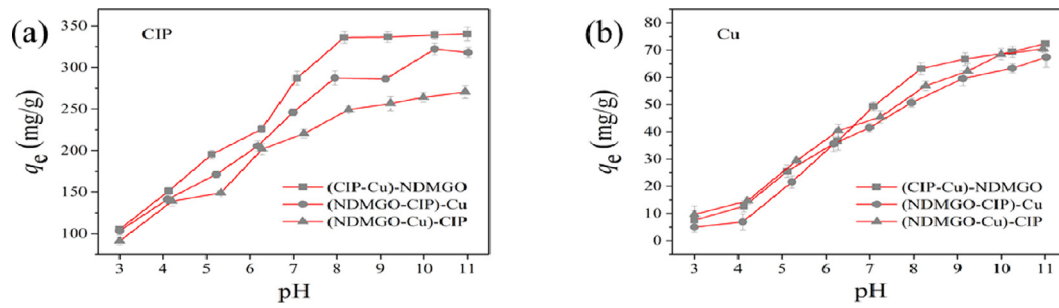


**Fig. 7.** pH effects for all three CIP/Cu(II) addition sequences on CIP (a) and Cu(II) (b) adsorption onto NDMGO.  $C_{0(\text{CIP})} = 50 \text{ mg/L}$ ,  $C_{0(\text{Cu})} = 10 \text{ mg/L}$ ,  $m/V = 0.10 \text{ g/L}$ ,  $T = 25^\circ\text{C}$ ,  $t = 14 \text{ h}$ .

tem, Cu(II) was pre-equilibrated with NDMGO, when CIP was added to the suspension of NDMGO–Cu(II), strong complexation between CIP and unadsorbed Cu(II) would stabilize Cu(II) in solution, thereby more Cu(II) ions were adsorbed on NDMGO than in the (NDMGO–CIP)–Cu(II) systems in all the studied pH ranges. In the case of (CIP–Cu(II))–NDMGO, the adsorption capacity of Cu(II) was between that of (NDMGO–Cu(II))–CIP and (NDMGO–CIP)–Cu(II) systems at  $\text{pH} < 6.5$ , whereas the Cu(II) removal showed a higher efficiency than in the other two ternary systems at  $\text{pH} > 6.5$ . The speciation of the CIP and Cu(II) over the pH range 3.0–11.0 are illustrated in Figs. S1 and S2, respectively. At  $\text{pH} < 6.5$ , free  $\text{Cu}^{2+}$ ,  $\text{Cu}_2(\text{OH})_2^{2+}$ , and  $\text{CuOH}^+$  were the dominant complex species, and the positive  $\text{Cip}^+$  ions would compete the sorption sites with the three possible species on the surfaces of NDMGO. Above pH 6.5, the increase of removal capacities of Cu(II) in the (NDMGO–CIP)–Cu(II) systems might cause by the formation of the precipitation of  $\text{Cu}(\text{OH})_2(\text{s})$ . According to the above analyses of Cu(II) and CIP adsorption on the systems formed via three different addition sequences, we could conclude that the CIP and Cu(II) adsorption on NDMGO was controlled by both soluble CIP or Cu(II) in the solution and surface-adsorbed CIP or Cu(II). Beyond that, it was also dependent on the solution pH for all three CIP/Cu(II) addition.

### 3.7. Adsorption mechanism

In order to investigate the adsorption mechanism, XPS and FI-IR analyses were usually performed by identifying the chemical ele-

ments on the surface of the adsorbent. XPS survey scans of CIP and CIP/Cu before and after adsorption on NDMGO are presented in Fig. S4. Three major elements including C, N and O were observed on NDMGO, NDMGO–CIP, and NDMGO–CIP/Cu surface. The minor amounts of F and Cu indicated that the CIP and Cu(II) were partially adsorbed. The adsorption mechanism was studied as follows:

The N 1s peaks of the NDMGO before and after adsorption CIP could be resolved into three peaks (Fig. 8a and b). Fig. 8a showed the binding energy and percentage of the three peaks for NDMGO, including 59.65% of  $-(\text{CH}_2)_3\text{N}$  at 399.61 eV, 26.90% of  $-\text{NH}/\text{C}-\text{N}$  at 401.19 eV and 14.26% of  $\text{N}^+$  at 401.72 eV [38,39]. When CIP adsorbed onto the surface of NDMGO (Fig. 8b), the percentage of  $\text{N}^+$  increased obviously from 14.26% to 31.42% and the  $-(\text{CH}_2)_3\text{N}$  increased from 59.65% to 63.76%, while the  $-\text{NH}/\text{C}-\text{N}$  decreased from 26.90% to 4.83%, suggested that the amino groups should be responsible for the adsorption process [38]. The computer deconvolution XPS spectra of O 1s are shown in Fig. 8d–f. Before adsorption, the O 1s spectrum of NDMGO was deconvoluted into three peaks at 530.17, 531.47 and 533.32 eV, corresponding to the  $\text{Fe}-\text{O}$  ( $\text{Fe}_3\text{O}_4$ ), C–O (alcoholic hydroxyl and ether), and C=O groups, respectively [22,40]. After CIP adsorption, the molar ratio of the C=O increased from 22.85% to 41.31% and the molar ratio of the C–O reduced from 39.73% to 31.75%. These changes indicated that the oxygen-containing functional groups (hydroxyl and carboxyl groups) of NDMGO might be combined with the carbonyl and carboxyl groups of CIP. Thus hydrogen bond might play a role in the

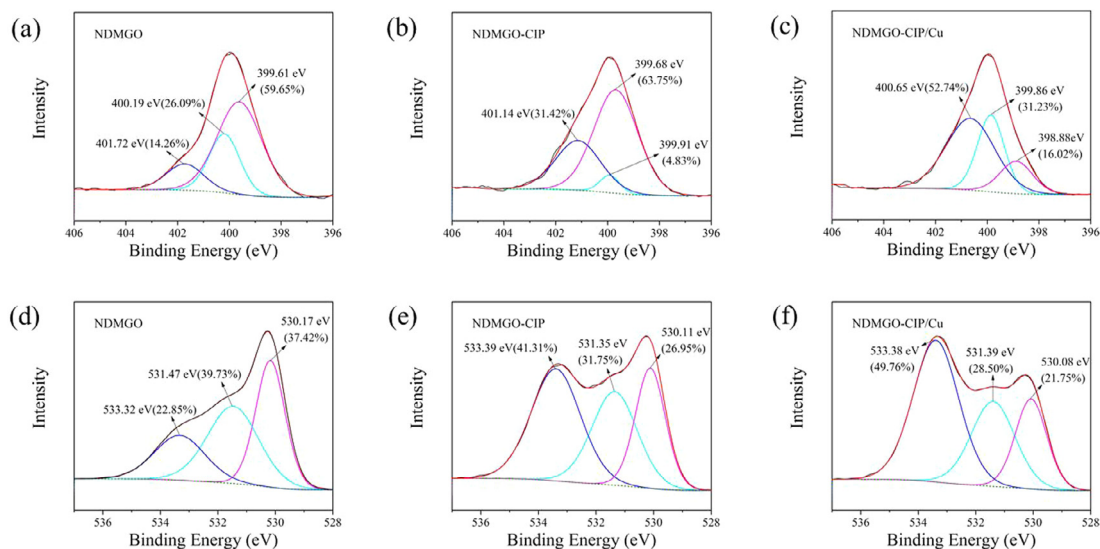


**Fig. 8.** (a), (b) and (c) are the computer deconvolution N 1s spectra of NDMGO, NDMGO–CIP and NDMGO–CIP/Cu, respectively; (d), (e) and (f) are the computer deconvolution O 1s spectra of NDMGO, NDMGO–CIP and NDMGO–CIP/Cu, respectively.

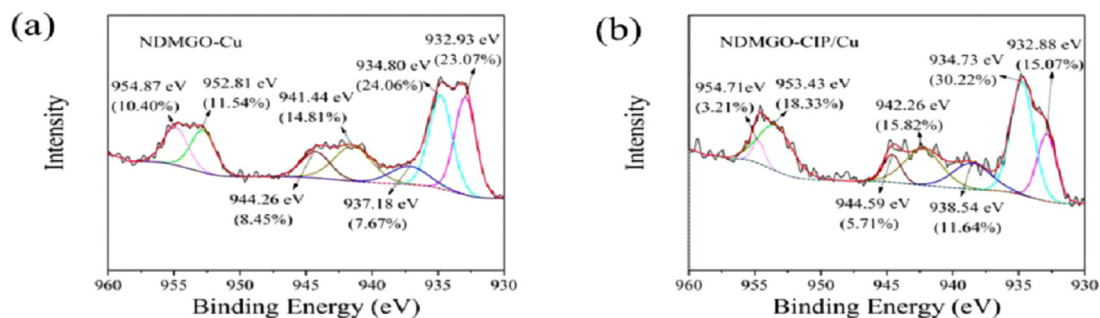


Fig. 9. (a) and (b) are the computer deconvolution Cu2p spectra of NDMGO-Cu and NDMGO-CIP/Cu, respectively.

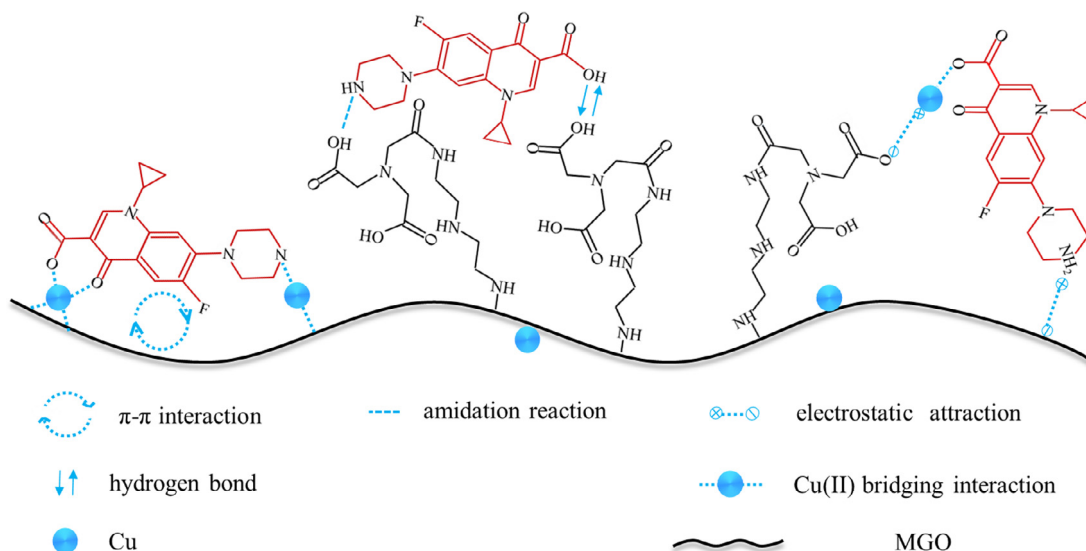


Fig. 10. Schematic illustration of CIP adsorption mechanism by NDMGO.

adsorption process [19]. According to the FT-IR analysis (Fig. 1d), after CIP uptake, two peaks at 3442 and 1398  $\text{cm}^{-1}$  belonged to the O–H and O=C–O stretching vibration presented a shift to 3469 and 1390  $\text{cm}^{-1}$ , respectively. Therefore, the oxygen-containing functional groups might provide the adsorption sites for CIP adsorption, which was in good agreement with XPS results. Moreover, the peaks belonged to the skeletal vibration of C=C bonds shifted from 1641 to 1621  $\text{cm}^{-1}$  after adsorption of CIP. It was confirmed that the  $\pi$ - $\pi$  interaction between CIP and NDMGO might be one of the most important adsorption driving forces [23].

From the above experimental results, the sorption amounts of CIP or Cu(II) on NDMGO were increased markedly when CIP/Cu coexisted in the aqueous solution. This might be attributed to a part of Cu(II) was combined with the CIP, and acted as a bridge between Cu(II) and CIP. This mechanism could be explained by the FT-IR and XPS spectra analyses. Fig. 1d showed the FT-IR spectra of NDMGO, NDMGO-Cu, and NDMGO-CIP/Cu. After the adsorption of Cu(II) onto NDMGO, the adsorption peak (at 1458  $\text{cm}^{-1}$ ) belonged to N–H disappeared and the peak corresponding to O–H and O=C–O migrated from 3442 and 1398  $\text{cm}^{-1}$  to 3429 and 1384  $\text{cm}^{-1}$ , respectively. When CIP/Cu adsorbed onto NDMGO, the peak of O–H, O=C–O, and N–H groups also slightly shifted. The changes in FT-IR spectra confirmed that the complexation occurred between Cu(II) and oxygen-containing and nitrogen-containing functional groups located in the adsorbent and CIP. The XPS spectrum of the NDMGO nanocomposite after Cu(II) adsorption (Fig. 9a) could be fitted to seven peaks at binding energy of 932.93, 934.80, 937.18, 941.44, 944.26, 952.81 and 954.87 eV. The peak at 934.80 eV (Cu 2p<sub>3/2</sub>) might be attributed

to the complexes of –NH<sub>2</sub>–Cu(II) or –NH–Cu(II) [41], and its molar ratio increased from 24.06% to 30.22% when CIP coexisted in this system, which further proved the interaction of Cu(II) with amino groups in CIP to form CIP–Cu(II) complexes. And the peak at 954.87 eV (Cu 2p<sub>1/2</sub>) was assigned to the purely physical Cu(II) adsorption [42]. Moreover, a satellite band (937.18–944.59 eV) nearby the Cu 2p<sub>3/2</sub> peak was representative of the oxidation state of Cu(II) [38], which indicated that the Cu(II) existed on the NDMGO through forming the Cu<sup>2+</sup>–O coordinate bonds. From the XPS spectra of N 1s and O 1s of NDMGO-CIP/Cu (Fig. 8c and f), the molar ratio of the N<sup>+</sup> and C=O peaks increased to 52.74% and 49.76%, and the –(CH<sub>2</sub>)<sub>3</sub>N and C–O peaks decreased to 16.02% and 28.50%, respectively, compared with that of NDMGO-CIP. Above results, together with binding energy shift, could be confirmed that Cu(II) ions could chelate with N or O atoms of CIP to form CIP–Cu(II) complex. The same adsorption mechanism was also reported in the previous literatures [41,42]. In addition to the Cu(II) bridge interaction, the CIP linked to positively charged Cu(II) had stronger sorption affinity to negatively charged NDMGO than the isolated CIP, and thus Cu(II) and CIP adsorption onto NDMGO was involved in electrostatic interaction. From the above analysis and discussion, the adsorption mechanism of Cu(II) and CIP onto NDMGO was schematically illustrated in Fig. 10.

#### 4. Conclusion

In this work, the NDMGO exhibited excellent sorption capacity for CIP and could be easily separated and recycled via an external magnet from treated solution after adsorption. The results implied

that the adsorption process of CIP was better presented by the pseudo-second-order model. Furthermore, the isotherm adsorption data were well described by the Freundlich model and the adsorption obeyed a spontaneous and endothermic process. When CIP and Cu(II) coexisted in the solution, the adsorption capacity of CIP was significantly enhanced due to the bridge enhancement where Cu(II) could provide additional sites to coordinate with N and O atoms of CIP. Besides, the XPS and FT-IR analyses showed that electrostatic attraction, hydrogen bonds,  $\pi$ - $\pi$  interaction, and amidation reaction were the critical driving force for this adsorption. This research highlighted the effects of Cu(II) concentrations and addition sequences. With the increase of Cu(II) concentrations, some greatly positive influence was gradually exerted. In the (CIP-Cu(II))-NDMGO system, CIP could pre-equilibrate with Cu(II) strongly via its carboxyl and keto groups, and more CIP molecules were adsorbed on NDMGO than in the ternary (NDMGO-Cu(II))-CIP and (NDMGO-CIP)-Cu(II) systems overall the pH values. Even more interesting was that background electrolyte and ionic strength presented a significant effect on the removal of CIP in the presence or absence of Cu(II). Findings from this work indicated that NDMGO could serve as a promising adsorbent for wastewaters containing both inorganic and organic pollutants from aqueous solutions.

## Acknowledgements

This research was financially supported by the National Natural Science Foundation of China (Grant Nos. 51609268, 51521006 and 51608208), the International S&T Cooperation Program of China (Project Contract No. 2015DFG92750), the Guangdong Natural Science Foundation (Grants No. 2016A030310246), and the Science and Technology Planning Project of Hunan Province (Grant Nos. 2016SK2010 and 2016SK2001).

## Appendix A. Supplementary data

Supplementary data associated with this article can be found, in the online version, at <http://dx.doi.org/10.1016/j.cej.2017.03.016>.

## References

- [1] S. Shi, Y. Fan, Y. Huang, Facile low temperature hydrothermal synthesis of magnetic mesoporous carbon nanocomposite for adsorption removal of ciprofloxacin antibiotics, *Ind. Chem. Res.* 52 (2013) 2604–2612.
- [2] Y. Sun, Q. Yue, B. Gao, Y. Gao, X. Xu, Q. Li, Y. Wang, Adsorption and cosorption of ciprofloxacin and Ni(II) on activated carbon-mechanism study, *J. Taiwan Inst. Chem. Eng.* 45 (2014) 681–688.
- [3] Y. Yan, S. Sun, Y. Song, X. Yan, W. Guan, X. Liu, W. Shi, Microwave-assisted in situ synthesis of reduced graphene oxide-BiVO<sub>4</sub> composite photocatalysts and their enhanced photocatalytic performance for the degradation of ciprofloxacin, *J. Hazard. Mater.* 250–251 (2013) 106–114.
- [4] X.F. Tan, S.B. Liu, Y.G. Liu, Y.L. Gu, G.M. Zeng, X.J. Hu, X. Wang, S.H. Liu, L.H. Jiang, Biochar as potential sustainable precursors for activated carbon production: multiple applications in environmental protection and energy storage, *Bioresour. Technol.* 227 (2017) 359–372.
- [5] Z. Pei, X.Q. Shan, J. Kong, B. Wen, G. Owens, Co-adsorption of ciprofloxacin and Cu(II) on montmorillonite and kaolinite as affected by solution pH, *Environ. Sci. Technol.* 44 (2009) 915–920.
- [6] X. Tan, Y. Liu, G. Zeng, X. Wang, X. Hu, Y. Gu, Z. Yang, Application of biochar for the removal of pollutants from aqueous solutions, *Chemosphere* 125 (2015) 70–85.
- [7] X.F. Tan, Y.G. Liu, Y.L. Gu, Y. Xu, G.M. Zeng, X.J. Hu, S.B. Liu, X. Wang, S.M. Liu, J. Li, Biochar-based nano-composites for the decontamination of wastewater: a review, *Bioresour. Technol.* 212 (2016) 318–333.
- [8] J. Ma, M. Yang, F. Yu, J. Zheng, Water-enhanced removal of ciprofloxacin from water by porous graphene hydrogel, *Sci. Rep.* 5 (2015) 13578.
- [9] X. Gu, Y. Tan, F. Tong, C. Gu, Surface complexation modeling of co-adsorption of antibiotic ciprofloxacin and Cu(II) and onto goethite surfaces, *Chem. Eng. J.* 269 (2015) 113–120.
- [10] M.F. Li, Y.G. Liu, G.M. Zeng, S.B. Liu, X.J. Hu, D. Shu, L.H. Jiang, X.F. Tan, X.X. Cai, Z.L. Yan, Tetracycline adsorbed onto nitrilotriacetic acid-functionalized magnetic graphene oxide: influencing factors and uptake mechanism, *J. Colloid Interface Sci.* 485 (2017) 269–279.
- [11] D.L. Huang, G.M. Zeng, C.L. Feng, S. Hu, X.Y. Jiang, L. Tang, F.F. Su, Y. Zhang, W. Zeng, H.L. Liu, Degradation of lead-contaminated lignocellulosic waste by *Phanerochaete chrysosporium* and the reduction of lead toxicity, *Environ. Sci. Technol.* 42 (2008) 4946–4951.
- [12] S. Liu, H. Wang, L. Chai, M. Li, Effects of single- and multi-organic acid ligands on adsorption of copper by Fe<sub>3</sub>O<sub>4</sub>/graphene oxide-supported DCTA, *J. Colloid Interface Sci.* 478 (2016) 288–295.
- [13] E. Mosayebi, S. Azizian, Study of copper ion adsorption from aqueous solution with different nanostructured and microstructured zinc oxides and zinc hydroxide loaded on activated carbon cloth, *J. Mol. Liq.* 214 (2016) 384–389.
- [14] Y.J. Wang, D.A. Jia, R.J. Sun, H.W. Zhu, D.M. Zhou, Adsorption and cosorption of tetracycline and copper(II) on montmorillonite as affected by solution pH, *Environ. Sci. Technol.* 42 (2008) 3254–3259.
- [15] Y. Yao, S. Miao, S. Liu, L.P. Ma, H. Sun, S. Wang, Synthesis, characterization, and adsorption properties of magnetic Fe<sub>3</sub>O<sub>4</sub>@graphene nanocomposite, *Chem. Eng. J.* 184 (2012) 326–332.
- [16] T.S. Sreeprasad, S.M. Maliyekkal, K.P. Lisha, T. Pradeep, Reduced graphene oxide-metal/metal oxide composites: facile synthesis and application in water purification, *J. Hazard. Mater.* 186 (2011) 921–931.
- [17] X.J. Hu, Y.G. Liu, H. Wang, A.W. Chen, G.M. Zeng, S.M. Liu, Y.M. Guo, X. Hu, T.T. Li, Y.Q. Wang, L. Zhou, S.H. Liu, Removal of Cu(II) ions from aqueous solution using sulfonated magnetic graphene oxide composite, *Sep. Purif. Technol.* 108 (2013) 189–195.
- [18] X. Hu, H. Wang, Y. Liu, Statistical analysis of main and interaction effects on Cu(II) and Cr(VI) decontamination by nitrogen-doped magnetic graphene oxide, *Sci. Rep.* 6 (2016) 34378.
- [19] S. Wu, X. Zhao, Y. Li, C. Zhao, Q. Du, J. Sun, Y. Wang, X. Peng, Y. Xia, Z. Wang, L. Xia, Adsorption of ciprofloxacin onto biocomposite fibers of graphene oxide/calcium alginate, *Chem. Eng. J.* 230 (2013) 389–395.
- [20] X.J. Hu, Y.G. Liu, H. Wang, G.M. Zeng, X. Hu, Y.M. Guo, T.T. Li, A.W. Chen, L.H. Jiang, F.Y. Guo, Adsorption of copper by magnetic graphene oxide-supported  $\beta$ -cyclodextrin: effects of pH, ionic strength, background electrolytes, and citric acid, *Chem. Eng. Res. Des.* 93 (2015) 675–683.
- [21] H. Wang, Y.G. Liu, G.M. Zeng, X.J. Hu, X. Hu, T.T. Li, H.Y. Li, Y.Q. Wang, L.H. Jiang, Grafting of  $\beta$ -cyclodextrin to magnetic graphene oxide via ethylenediamine and application for Cr(VI) removal, *Carbohydr. Polym.* 113 (2014) 166–173.
- [22] N.A. Travlou, G.Z. Kyzas, N.K. Lazaridis, E.A. Deliyanni, Functionalization of graphite oxide with magnetic chitosan for the preparation of a nanocomposite dye adsorbent, *Langmuir* 29 (2013) 1657–1668.
- [23] L.H. Jiang, Y.G. Liu, G.-M. Zeng, F.Y. Xiao, X.J. Hu, X. Hu, H. Wang, T.T. Li, L. Zhou, X.F. Tan, Removal of 17 $\beta$ -estradiol by few-layered graphene oxide nanosheets from aqueous solutions: external influence and adsorption mechanism, *Chem. Eng. J.* 284 (2016) 93–102.
- [24] L. Jiang, Y. Liu, S. Liu, X. Hu, G. Zeng, X. Hu, S. Liu, S. Liu, B. Huang, M. Li, Fabrication of  $\beta$ -cyclodextrin/poly (l-glutamic acid) supported magnetic graphene oxide and its adsorption behavior for 17 $\beta$ -estradiol, *Chem. Eng. J.* 308 (2017) 597–605.
- [25] X. Peng, F. Hu, H. Dai, Q. Xiong, C. Xu, Study of the adsorption mechanisms of ciprofloxacin antibiotics onto graphitic ordered mesoporous carbons, *J. Taiwan Inst. Chem. Eng.* 65 (2016) 472–481.
- [26] Z. Fu, C. He, H. Li, C. Yan, L. Chen, J. Huang, Y.-N. Liu, A novel hydrophilic-hydrophobic magnetic interpenetrating polymer networks (IPNs) and its adsorption towards salicylic acid from aqueous solution, *Chem. Eng. J.* 279 (2015) 250–257.
- [27] C.L. Zhang, G.L. Qiao, F. Zhao, Y. Wang, Thermodynamic and kinetic parameters of ciprofloxacin adsorption onto modified coal fly ash from aqueous solution, *J. Mol. Liq.* 163 (2011) 53–56.
- [28] H. Chen, B. Gao, H. Li, Removal of sulfamethoxazole and ciprofloxacin from aqueous solutions by graphene oxide, *J. Hazard. Mater.* 282 (2015) 201–207.
- [29] Z.L. Yan, Y.G. Liu, X.F. Tan, S.B. Liu, G.M. Zeng, L.H. Jiang, M.F. Li, Z. Zhou, S. Liu, X.X. Cai, Immobilization of aqueous and sediment-sorbed ciprofloxacin by stabilized Fe-Mn binary oxide nanoparticles: influencing factors and reaction mechanisms, *Chem. Eng. J.* 314 (2017) 612–621.
- [30] X.J. Hu, Y.G. Liu, G.M. Zeng, H. Wang, X. Hu, A.W. Chen, Y.Q. Wang, Y.M. Guo, T. Li, L. Zhou, S.H. Liu, X.X. Zeng, Effect of aniline on cadmium adsorption by sulfanilic acid-grafted magnetic graphene oxide sheets, *J. Colloid Interface Sci.* 426 (2014) 213–220.
- [31] S. Yang, J. Hu, C. Chen, D. Shao, X. Wang, Mutual effects of Pb(II) and humic acid adsorption on multiwalled carbon nanotubes/polyacrylamide composites from aqueous solutions, *Environ. Sci. Technol.* 45 (2011) 3621–3627.
- [32] J. Li, S. Zhang, C. Chen, G. Zhao, X. Yang, J. Li, X. Wang, Removal of Cu(II) and fulvic acid by graphene oxide nanosheets decorated with Fe<sub>3</sub>O<sub>4</sub> nanoparticles, *Appl. Mater. Interfaces* 4 (2012) 4991–5000.
- [33] X.J. Hu, Y.G. Liu, G.M. Zeng, S.H. You, H. Wang, X. Hu, Y.M. Guo, X.F. Tan, F.Y. Guo, Effects of background electrolytes and ionic strength on enrichment of Cd(II) ions with magnetic graphene oxide-supported sulfanilic acid, *J. Colloid Interface Sci.* 435 (2014) 138–144.
- [34] M. Liu, C. Chen, J. Hu, X. Wu, X. Wang, Synthesis of magnetite/graphene oxide composite and application for cobalt(II) removal, *J. Phys. Chem. C* 115 (2011) 25234–25240.
- [35] S. Yang, G. Sheng, Z. Guo, X. Tan, J. Xu, X. Wang, Investigation of radionuclide <sup>63</sup>Ni(II) sequestration mechanisms on mordeite by batch and EXAFS spectroscopy study, *Sci. China Chem.* 55 (2011) 632–642.
- [36] K.F. Lam, X. Chen, G. McKay, K.L. Yeung, Anion effect on Cu<sup>2+</sup> adsorption on NH<sub>2</sub>-MCM-41, *Ind. Eng. Chem. Res.* 47 (2008) 9376–9383.

- [37] X.J. Hu, Y.G. Liu, G.M. Zeng, H. Wang, S.H. You, X. Hu, X.F. Tan, A.W. Chen, F.Y. Guo, Effects of inorganic electrolyte anions on enrichment of Cu(II) ions with aminated Fe<sub>3</sub>O<sub>4</sub>/graphene oxide: Cu(II) speciation prediction and surface charge measurement, *Chemosphere* 127 (2015) 35–41.
- [38] B. Huang, Y. Liu, B. Li, S. Liu, G. Zeng, Z. Zeng, X. Wang, Q. Ning, B. Zheng, C. Yang, Effect of Cu(II) ions on the enhancement of tetracycline adsorption by Fe<sub>3</sub>O<sub>4</sub>@SiO<sub>2</sub>-Chitosan/graphene oxide nanocomposite, *Carbohydr. Polym.* 157 (2017) 576–585.
- [39] S. Karthikeyan, M.A. Kumar, P. Maharaja, T. Partheeban, J. Sridevi, G. Sekaran, Process optimization for the treatment of pharmaceutical wastewater catalyzed by poly sulphate sponge, *J. Taiwan Inst. Chem. Eng.* 45 (2014) 1739–1747.
- [40] A.Z. Badruddoza, A.S. Tay, P.Y. Tan, K. Hidajat, M.S. Uddin, Carboxymethyl-beta-cyclodextrin conjugated magnetic nanoparticles as nano-adsorbents for removal of copper ions: synthesis and adsorption studies, *J. Hazard. Mater.* 185 (2011) 1177–1186.
- [41] Z.C. Wu, Z.Z. Wang, J. Liu, J.H. Yin, S.P. Kuang, A new porous magnetic chitosan modified by melamine for fast and efficient adsorption of Cu(II) ions, *Int. J. Biol. Macromol.* 81 (2015) 838–846.
- [42] W. Jiang, X. Chen, B. Pan, Q. Zhang, L. Teng, Y. Chen, L. Liu, Spherical polystyrene-supported chitosan thin film of fast kinetics and high capacity for copper removal, *J. Hazard. Mater.* 276 (2014) 295–301.